

Visible light photoluminescence in TiO₂/CdS nanopowders synthesized by sol-gel route: effect of gel aging time

E. S. Ulyanova¹, D. A. Zamyatin^{2,3}, V. Yu. Kolosov³, E. V. Shalaeva¹

¹Institute of Solid State Chemistry of Ural Branch of the Russian Academy of Sciences, Pervomayskaya, 91, Ekaterinburg, 620990, Russia

²Institute of Geology and Geochemistry of Ural Branch of the Russian Academy of Sciences, Vonsovskogo, 15, Ekaterinburg, 620075, Russia

³Ural Federal University named B. N. Yeltsin, Mira, 9, Ekaterinburg, 620002, Russia

tsivileva.yekaterina@yandex.ru, dzamyatin85@gmail.ru, Kolosov@urfu.ru, shalaeva@ihim.uran.ru

PACS 81.07.-b, 32.50.+d, 73.20.Hb

DOI 10.17586/2220-8054-2020-11-4-480-487

A series of sol-gel TiO₂/CdS, TiO₂ powders and coagulated CdS nanoparticles were studied by XRD, HRTEM and Raman spectroscopy to elucidate the effect of low-temperature gel aging time on visible photoluminescence (PL) emission of the TiO₂/CdS composites. With an increase in aging time a content of amorphous titania and incorporated CdS nanoparticles decreases in composites. For all composites, visible PL emission includes bands attributed to surface oxygen vacancies and hydroxyl group of TiO₂ nanocrystals, as well as yellow-green and red bands related to lattice defect states of CdS nanoparticles. It was found that gel aging time is a crucial parameter to influence visible PL emission in composites. This emission is suppressed with increasing aging time, and its evolution shows that healing of oxygen vacancy defects and hydroxyl group affect visible emission more significantly than improving crystallinity degree. The correlation between visible PL emission in TiO₂/CdS and their visible-light photocatalytic activity was discussed.

Keywords: TiO₂/CdS composites, nanoparticles, photoluminescence, defect states, sol-gel route.

Received: 20 August 2020

Revised: 24 August 2020

1. Introduction

Semiconductor TiO₂/CdS composites represent an important group of visible-light photoactive materials and are attracting considerable attention due to the fact that cadmium sulfide has a relatively narrow band gap and is well combined with the band structure of titanium dioxide [1–3]. The development of physical and chemical methods for the synthesis of nanoscale semiconductor particles and quantum dots has provided new possibilities for the creation of photoactive heterogeneous structures based on these phases. In nanosized systems, a more efficient carrier transfer takes place owing to the improved interface contacts [4, 5]. The efficiency of the photon energy conversion into photocurrent and the photocatalytic activity depend not only on a charge carrier transfer rate across the interface of the TiO₂/CdS couple but also on a recombination rate of the photogenerated electron-hole pair within titanium dioxide and CdS layers [2].

For visible-light photoactive nano-sized TiO₂/CdS composites [6–8], as well as for the visible photoactive TiO₂-doped materials [9, 10], the direct correlation has been often found between the increased photoactivity and decreased radiative recombination in the visible range. Visible-light emission, related to the radiative recombination in nanosized TiO₂ is mainly attributed to (I) the self-trapped excitons, (II) oxygen vacancies and (III) surface states [11–14]. For CdS nanocrystals and nanoparticles, visible PL includes a number of emission bands associated with both surface electron states and states of complex defect centers [15–18]. Visible PL emission is affected not only by surface and lattice defects of TiO₂ nanocrystals but their morphology [13], and as well as by the crystallinity degree of titania [19]. For TiO₂/CdS composites, recombination rate has been found to increase with increasing degree of defects in TiO₂ layers [20] and imperfection of TiO₂||CdS interface [5]. Concentration ratio of TiO₂:CdS is also an essential parameter which affects the visible PL emission, with the concentration dependence of PL emission being non-monotonic [6].

Currently, several synthesis strategies are being actively developed to obtain visible photoactive TiO₂/CdS nanocomposites, and by varying the synthesis conditions it is possible to change their structural properties, defect states and electron structure for tuning PL emission. In one of them, pre-synthesized CdS nanoparticles are directly incorporated into TiO₂ matrix during titania formation process via sol-gel route [21–24]. As a rule, the influence of the initial concentrations of the sensitizing additive on the emission and photocatalytic properties of sol-gel TiO₂/CdS composites is studied [21]. At the same time, when preparing TiO₂/CdS composites, the sol-gel route is sometimes used with low-temperature heating of the sol-gel [23,24], the effect of which on PL emission was not monitored. Recently, a new

technique for producing photoactive composites TiO₂/CdS was proposed, based on a modified sol-gel method using pre-synthesized CdS colloidal nanoparticles and low-temperature gel aging stage at boiling point [24]. Gel aging time, as has been shown, can affect the crystallinity degree of titania (amorphous/nanocrystalline ratio), and content of the incorporated CdS nanoparticles [25]. In addition, it must be taken into account that the stage of low-temperature gel aging promotes polycondensation of hydrolysis products to form titania and decrease of the oxygen vacancy and the hydroxyl group in synthesized titania [26].

The aim of work is to elucidate the effect of gel aging time on visible PL emission in TiO₂/CdS composites prepared by sol-gel route using pre-synthesized CdS nanoparticles and gel aging stage at boiling point. To gain more insight into the defect-related PL emission, a series of TiO₂/CdS and bare TiO₂ powders as well as CdS coagulated nanoparticles were studied. XRD, HRTEM and Raman spectroscopy were employed to characterize the structure of the samples and revealed decrease in content of amorphous TiO₂ and incorporated CdS nanoparticles with aging time. For all TiO₂/CdS composites, PL emission was found to include bands related to the surface defect states of TiO₂ nanocrystallites and two emission bands (as yellow-green and red), related to lattice defect states of CdS nanoparticles. Significant and non-additive growth of visible emission bands contributed by both phases was detected at the early aging stage and discussed in terms of TiO₂||CdS interface defects. The increase in gel aging time was demonstrated to be a crucial factor to suppress visible PL emission in TiO₂/CdS composites. It was concluded that the surface defects of TiO₂ and content of the incorporated CdS nanoparticles predominantly affect the visible emission, unlike the crystallinity degree of titania. A TiO₂/CdS composite with suppressed visible PL emission was found to exhibit the enhanced visible light photoactivity.

2. Experimental part

TiO₂/CdS composites were prepared by direct hydrolysis technique using pre-synthesized aqueous colloidal solution of CdS nanoparticles. The details of TiO₂/CdS preparation can be found in [24]. In brief, a certain amount of titanium (IV) n-butoxide was dissolved in the aqueous colloidal CdS solution. Sol-gel samples were heated up to the boiling point under continuous stirring and aged at this temperature for 1, 3 and 4 h. To remove the remaining organic species, the powders were centrifuged and dried in air at 120°C for 3 h. Bare TiO₂ powders were also prepared by the same hydrolysis route in the pure deionized water. The aging time at boiling point was 1 and 4 h.

X-ray diffraction (XRD), high resolution transmission electron microscopy (HRTEM) and Raman micro-spectroscopy in resonance and off-resonance modes were employed to study structural state of TiO₂/CdS composites. The XRD patterns of samples were recorded by a Shimadzu MAXima-X XRD-7000 (Shimadzu, Japan) automatic diffractometer with CuK α radiation ($\lambda = 1.5406 \text{ \AA}$) in 2θ angle range 10–80° with a step 0.03° and an exposure time of 10 sec at each step. The volume fractions and structural characteristics of constituent phases were calculated employing PCW 2.4 software [27]. High resolution TEM images and electron diffraction patterns were obtained with the help of a JEM-2100 microscope (JEOL, Japan) equipped with an Energy Dispersive X-ray Analyzer (EDX). HRTEM images were processed with the Digital Micrograph software package. Raman and photoluminescence spectra were excited by a low-power (up to 10 mW) laser irradiation at wave length of 480, 514 and 633 nm at room temperature, and they were recorded by a LabRAM HR800 (Horiba, Japan) spectrometer, providing a focal spot on the samples of 1 – 2 μm diameter. The spectral resolution was about 1 cm^{-1} . Raman and photoluminescence spectra were analyzed with multi-peak Gaussian fitting method using the “Peakfit v 4.11” software package.

3. Results and discussion

3.1. Structure characterization of TiO₂/CdS composites

Figure 1(a) shows XRD patterns for TiO₂/CdS powder composites synthesized by sol-gel technique with varying gel aging time at boiling point. Curve fitting of XRD spectra indicates that all the samples contain anatase and brookite titanium dioxide phases with the approximate ratio 2:1. The average crystal sizes in powders, as estimated by Debye–Scherrer equation, change slightly with aging time and are equal to 6 – 7 nm for the sample TiO₂/CdS at the early aging time and about 7 – 8 nm for the sample with a deeper aging (3 or 4 h). According to HRTEM, the samples contain amorphous titanium dioxide, the concentration of which decreases from 15% to less than 5% with an increase in gel aging time. In the XRD spectra, in addition to dioxide titanium diffraction peaks there are the blurred diffraction peaks at 26.1, 43.5 and 51.0 degrees that can be attributed to CdS nanoparticles with randomly lattice-packed hexagonal structure [28]. The bare CdS nanoparticles coagulated from the initial colloidal solution exhibit similar crystalline structure. The sizes of incorporated CdS nanoparticles are 5-7 nm, which are close to those in the initial colloid solution characterized by the log-normal size distribution of particles with the average value of 4.5 nm [29]. Estimations made by Peakfit decomposition of XRD spectra showed that CdS nanoparticles concentration decreases with increasing gel aging time and is 9, 2 – 3 and about 1% CdS for TiO₂/CdS samples with 1, 3 and 4 h

aging, respectively. This effect was discussed in detail using the Molecular Dynamic simulations in our previous work [26]. The drop in the concentration of CdS nanoparticles is associated with the decreases in the content of the amorphous phase in the TiO_2 matrix and the calculated thermodynamic stability of the composite CdS @ TiO_2 nanoparticles depending on the structure of the titanium shell: amorphous titania > polycrystalline titania (anatase or brookite). HRTEM images confirmed that colloidal CdS nanoparticles are incorporated into all anatase/brookite matrices [26]. A typical HRTEM image of the incorporated CdS nanoparticle with zone axis [001] is given in the Fig. 1(b).

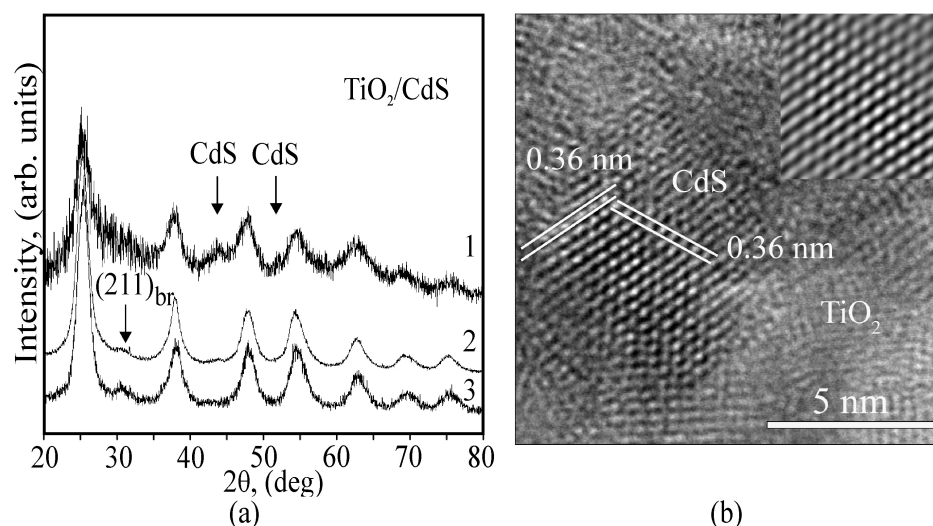


FIG. 1. X-ray diffraction patterns for the sol-gel TiO_2/CdS composites synthesized with varying gel aging time. The lines (1), (2) and (3) correspond to 1, 3 and 4 hours of aging (a). HRTEM image of a CdS nanoparticle incorporated into the TiO_2 matrix, [001] zone axis. The filtered image is presented in the inset (b)

A series of the micro-Raman spectra recorded from the different regions of powders demonstrates the good uniformity of structural properties of all synthesized samples TiO_2/CdS . Fig. 2 presents the typical untreated and treated Raman spectra for the TiO_2/CdS powders recorded with wavelength excitation equal to 633 nm. The most intense peaks in the treated spectra belong to titania phases (anatase and brookite). All 6 active modes of anatase phase (149 (E_{1g}), 200 (E_{2g}), 640 (E_{3g}), 401 ($B_{1g(1)}$), 517 cm^{-1} (A_{1g} and $B_{1g(2)}$)) can be detected for powders. There are weaker peaks which can be attributed to the modes of brookite phase [30]. These peaks are 128 (A_{1g}), 166 (A_{1g}), 218 (B_{1u}), 245 (A_{1g}), 323 (B_{1g}), 366 (B_{2g}) and 622 (B_{1u}) cm^{-1} . It can be seen that the corresponding peaks are shifted to the higher frequencies and smeared as compared to that of standard microcrystalline TiO_2 -anatase, indicating that the size effect for nanocrystals takes place. For all TiO_2/CdS powders, including powder with CdS concentration about 1%, in Raman spectra excited at 633 nm (1.95 eV), there is a smeared band with maximum around 300–302 cm^{-1} which becomes stronger for laser wavelength of 514 nm at resonance condition and can be uniquely assigned to the first longitudinal optical (LO) mode of CdS [31].

XRD, HRTEM and Raman spectroscopy revealed that all TiO_2/CdS composite powders have an anatase / brookite matrix with a phase ratio close to 2:1 and a small content of amorphous titanium dioxide. With an increase in the gel aging time at boiling point, the content of the amorphous component decreases from 15 to 5%, and the average crystallite size of the anatase and brookite phases increases slightly from 6.5 to 8 nm. The CdS particles incorporated into the TiO_2 matrix have an average size of approximately 5–7 nm, which is close to the average particle size in the initial CdS colloidal solution. The structure of the incorporated particles, as in the initial solution, is characterized by a random hexagonal close-packed lattice.

3.2. Photoluminescence properties of TiO_2/CdS composites

The inset in Fig. 2(a) presents the untreated Raman spectra recorded with a 633 nm excitation wavelength. As can be seen, with a decrease of gel aging time the untreated spectra demonstrate consistently increasing background due to visible light luminescence. In order to investigate the effects of luminescence and their aging time dependence in more detail, Raman spectra were recorded with a 480 nm excitation wavelength for TiO_2/CdS composites, CdS nanoparticles coagulated from the colloidal initial solution and bare TiO_2 powder synthesized by the same sol-gel

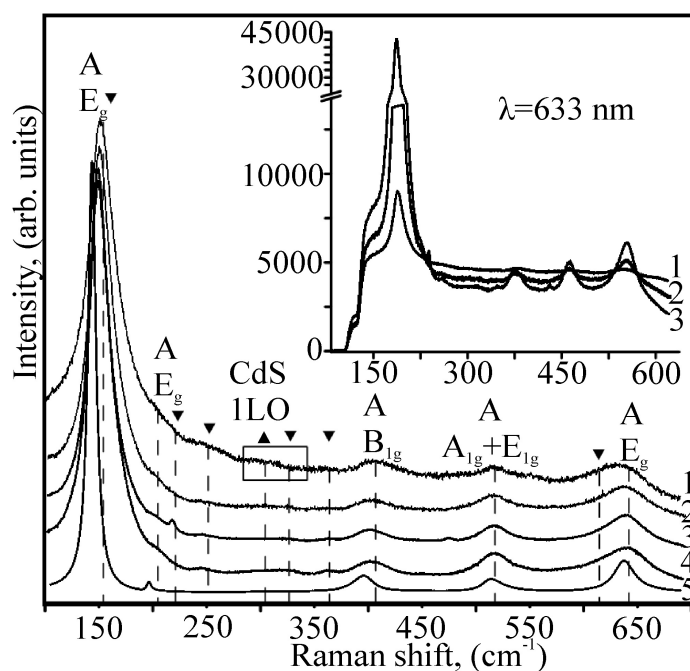


FIG. 2. Raman spectra for the sol-gel TiO₂/CdS (1, 2, 3), bare TiO₂ (4) nanopowders and microcrystalline anatase (5), excitation is 633 nm. The peaks of anatase (A) are signed. The peaks of CdS and brookite are marked with triangles and upside-down triangles, respectively. Notations (1, 2, 3) are the same as on Fig. 1(a). The untreated spectra are shown in insert

route with varying gel aging time. Deconvolution of the peaks was performed to gain more insight into the nature of defect states which determine the observed luminescence in different samples.

At first, consider the PL spectra of the bare TiO₂ nanopowder and CdS nanoparticles. Fig. 3(a,b) demonstrate visible light and NIR (near infrared) PL emission for the bare TiO₂ nanopowder synthesized with gel aging time of 1 and 4 h. For both sample, broad visible PL emission can be fitted with four Gaussian sub-band centered at 533 nm (2.3 eV), 580 nm (2.1 eV), 633 nm (1.95 eV) and 670 nm (1.85 eV). One band at 850 nm (1.46 eV) is observed in NIR region. The all visible emission bands can be associated to the radiative recombination at the surface defects sites such as oxygen vacancy and hydroxyl groups which are the dominant trapped sites for nano-powders fabricated by low-temperature sol-gel. One set visible emissions at 2.3 and 1.95 eV are attributed to the deexcitation from the lower levels of oxygen vacancies associated with Ti³⁺ in anatase lattice to the ground state [12, 14]. The sub-band at 2.1 eV is due to the deexcitation from lower levels in Ti³⁺ 3d states of TiO₂ lattice to the deep levels created by OH⁻ group [12]. The observed NIR PL emission at 1.46 eV is a signature of the brookite phase and appears due to the radiative recombination at the intrinsic lattice defects acting as trapped sites [32]. As a consequence of the fabrication process (sol-gel route), we can suppose that visible emission appears owing to the surface oxygen vacancies in brookite nanoparticles, and one additional sub-band centered at 1.85 eV is attributed to these defects.

For bare TiO₂ nanopowders, the intensity of all sub-bands of the visible light PL emission noticeably decreases with the increasing gel aging time at boiling point. Therefore, the changes in the surface defect concentrations in TiO₂ nano-powder with gel aging time significantly affect the visible PL emission, unlike the phase transformation of amorphous TiO₂ into a crystalline state which proceeds during the aging stage. In the latter case, the intensity of PL emission should have increased with the increases in the content of the crystalline phase [19].

A PL emission spectrum for CdS nanoparticles coagulated from the colloidal solution is presented in Fig. 3(c). A broad sub-band centered at 540 nm (2.3 eV) and a shoulder at 710 nm (1.75 eV) extended up to 940 nm (1.3 eV) are revealed. A similar PL band structure was observed earlier for CdS nanopowder which exhibits a structure related to that of CdS coagulated nanoparticles and is characterized by a high concentration of lattice stacking faults [17]. The yellow-green emission at 540 nm can be endorsed to the deexcitation from the Cd interstitial states to the valence band [15, 17, 18], and the red emission shoulder is believed to be caused by transitions of electrons trapped in the surface states to the valence band and to be increased with the accumulation of crystallographic defects in CdS structure [18].

Figure 3(d-f) demonstrates PL emission spectra for TiO₂/CdS composites fabricated by sol-gel using pre-synthesized CdS colloidal nanoparticles and with varying gel aging. The PL spectra of TiO₂/CdS composites managed to

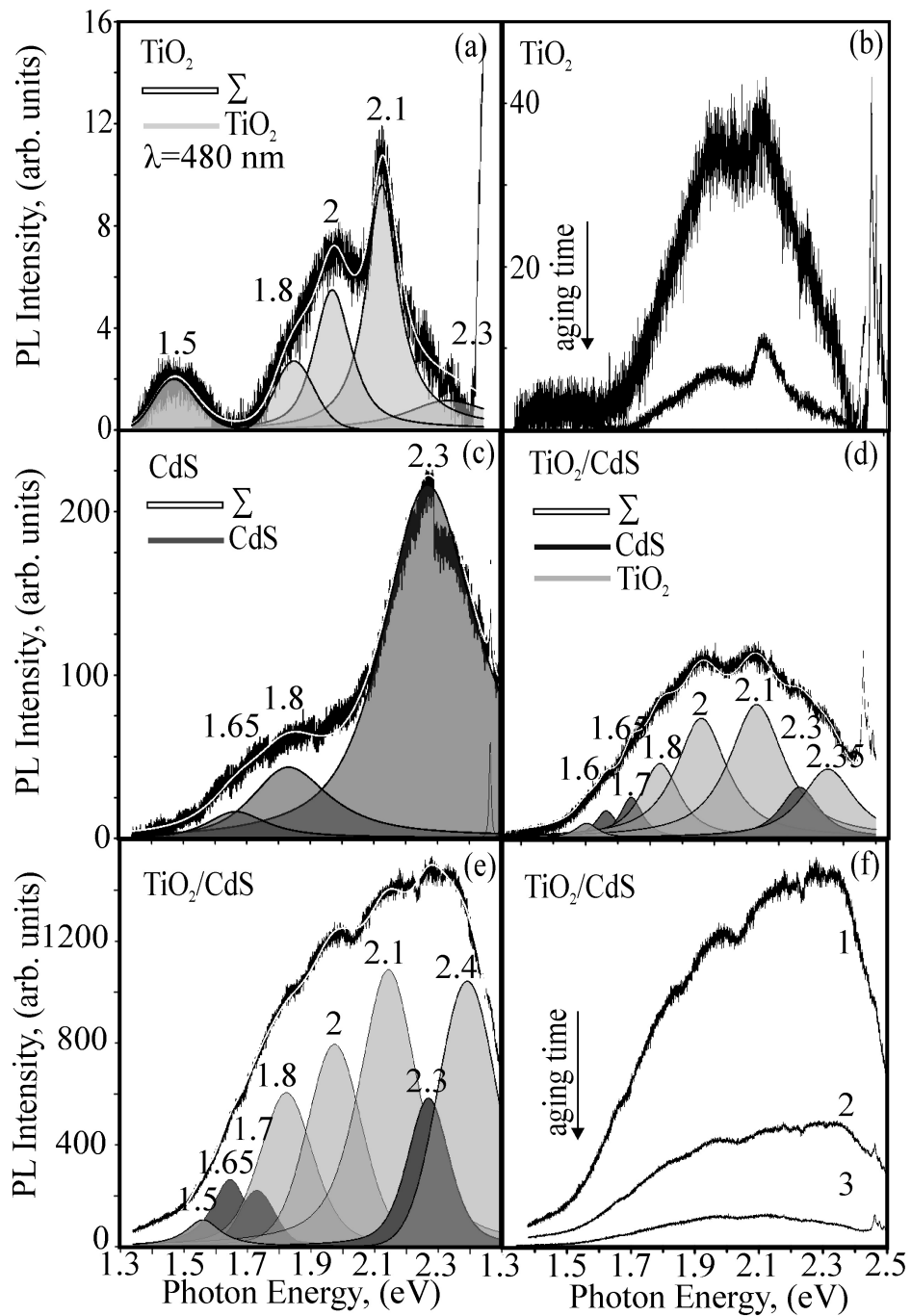


FIG. 3. PL emission for sol-gel TiO_2 (a,b), coagulated CdS nanoparticles (c) and sol-gel TiO_2/CdS nanopowders (d-f), excitation is 480 nm. For TiO_2 , gel aging time is 1 and 4 hours. For TiO_2/CdS , notations (1, 2, 3) are the same as on Fig. 1(a)

be decomposed by the same sub-bands as in bare TiO₂ nanopowder and CdS particles, with sub-band positions being changed slightly. The main difference in the spectra recorded for TiO₂/CdS powders with 1, 3 and 4 hours of gel aging stage is the decrease in the intensity of all emission sub-bands related to both the TiO₂ matrix and the incorporated CdS nanoparticles, with increasing gel aging time. As in the case of pure TiO₂, the effect of the phase transformation from amorphous TiO₂ to crystalline phases, which occurs during gel aging, on the emission of TiO₂/CdS composite powders is insignificant. In samples with short aging time (1 h) and containing the maximum amount of CdS nanoparticles up to 9%, visible emission is maximum, and is significantly higher than in the original pure components. As shown above and discussed in detail in our previous work [26], there are no significant differences between the structural properties of the components of the TiO₂/CdS composite and the original bare sol-gel TiO₂ nano-powder and CdS nanoparticles. However, the increased defect concentrations in the TiO₂/CdS interface region, detected by MD simulations of CdS @ TiO₂ composite particles, will affect surface defect states and lead to an increased visible PL emission, especially in the early stages of aging. With an increase in the aging time to 4 hours, PL emission drops significantly due to the decrease in the content of incorporated CdS nanoparticles to 1% and due to the healing of TiO₂/CdS interface defects and surface defects of TiO₂ nanocrystallites as in the case of the bare TiO₂ nanopowder.

Consider the relation between the observed visible PL emission for TiO₂/CdS powders synthesized with varying gel aging time and their visible light photocatalytic activity, previously tested in the oxidative degradation of benzene-1,4-diol (hydroquinone) [24]. Fig. 4 shows the rates of the oxidation reaction of benzene-1, 4-diol, the intensity of PL sub-band at 580 nm (2.1 eV) attributed to the surface hydroxyl group and content of CdS nanoparticles incorporated into TiO₂ matrix. It can be seen that the highest photoactivity is exhibited by composites with the lowest visible PL emission and the lowest CdS nanoparticle content. For a composite with short aging time and increased CdS content, a delayed decrease in photoactivity is observed, seemingly due to the competition of several alternative effects – (I) an increase in visible PL emission associated with harmful radiative recombination at the surface defect states, (II) an increase in the number of TiO₂||CdS heterojunctions which can improve the transfer and separation of charge carriers and (III) an increase in the number of titania surface defects serving as centers of photo-induced redox reactions.

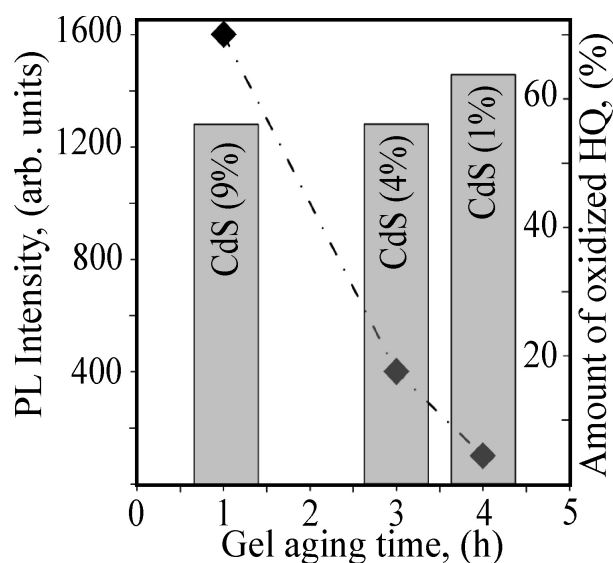


FIG. 4. Correlation dependences between the rate of hydroquinone (HQ) oxidation [24], PL emission related to the surface hydroxyl group and content of the incorporated CdS nanoparticles in the TiO₂/CdS nanopowders synthesized with varying gel aging time (1, 3 and 4 hours)

4. Conclusions

The paper explores the effect of gel aging time on visible light photoluminescence of TiO₂/CdS composites fabricated by modified sol-gel route using pre-synthesized CdS colloidal nanoparticles. For this, a series of TiO₂/CdS and bare TiO₂ powders prepared with varying gel aging time as well as bare CdS coagulated nanoparticles were studied. TiO₂/CdS and TiO₂ exhibit an amorphous-nanocrystalline structure, and with an increase in gel aging time, the content of amorphous titania decreases as phase transformation from amorphous into crystalline titania proceeds and the content of incorporated CdS nanoparticles decreases.

It was found that for sol-gel TiO₂/CdS powders, gel aging time at boiling point is a crucial parameter to affect visible light PL emission. With increasing aging time, visible PL emission associated with TiO₂ surface defects such as oxygen vacancy and hydroxyl group as well as yellow-green and red emission is suppressed, related to the defect states of CdS nanoparticles. At short aging times, a significant non-additive increase in the intensity of visible luminescence bands of both phases is observed, which is considered as a result of the increased structural imperfection in the TiO₂||CdS interface, especially at the early stages of aging. Surface defect states and concentration of CdS nanoparticles are concluded to significantly affect visible PL emission, unlike the crystallinity degree of titania.

There is a correlation between visible PL emission and visible-light photoactivity of TiO₂/CdS composites. Composites with suppressed visible PL emission exhibit the enhanced visible-light photoactivity.

Acknowledgements

The research was carried out in accordance with the state assignment for ISSC UB RAS and financial support from ISSC UB RAS (theme AAAA-A19-119031890025-9). TEM study was supported by RFBR (grant No. 20-02-00906). The authors are grateful to Dr. Kozhevnikova N. S. and Dr. Gorbunova T. I. for the provided samples TiO₂/CdS and CdS.

References

- [1] Vogel R., Honyer P., Weller H. Quantum-sized PbS, CdS, Ag₂S, Sb₂S₃, and Bi₂S₃ particles as sensitizers for various nanoporous wide-bandgap semiconductors. *J. Phys. Chem.*, 1994, **98**, P. 3183–3188.
- [2] Zhao D., Yang C.-F. Recent advances in the TiO₂/CdS nanocomposite used for photocatalytic hydrogen production and quantum-dot-sensitized solar cells. *Renewable and sustainable energy reviews*, 2016, **54**, P. 1048–1059.
- [3] Wang Y., Wang Q., Zhan X., Wang F., Safdar M., He J. Visible light driven type II heterostructures and their enhanced photocatalysis properties: a review. *Nanoscale*, 2013, **5**(18), P. 8326–8339.
- [4] He D., Chen M., Teng F., Li G., Shi H., Wang J., Xu M., Lu T., Ji X., Lv Y., Zhu Y. Enhanced cyclability of CdS/TiO₂ photocatalyst by stable interface structure. *Superlattices and Microstructures*, 2012, **51**, P. 799–808.
- [5] Zhang B., Zheng J., Li X., Fang Y., Wang L.-W., Lin Y. Pan F. Tuning band alignment by CdS layers using a SILAR method to enhance TiO₂/CdS/CdSe quantum-dot solar-cell performance. *Chem. Comm.*, 2016, **52**, P. 5706–5709.
- [6] Xie Z., Liu Z., Wang W., Liu C., Li Z. Zhang Z. Enhanced photoelectrochemical properties of TiO₂ nanorod arrays decorated with CdS nanoparticles. *Sci. Technol. Adv. Mater.*, 2014, **15**(5), P. 055006.
- [7] Huo Y., Yang X., Zhu J., Li H. Highly active and stable CdS-TiO₂ visible photocatalyst prepared by in situ sulfurization under supercritical conditions. *Appl. Catalysis B: Environmental*, 2011, **106**, P. 69–75.
- [8] Zhao H., Cui S., Yang L., Li G., Li N., Li X. Synthesis of hierarchically meso-macroporous TiO₂/CdS heterojunction photocatalysts with excellent visible-light photocatalytic activity. *Journal of Colloid and Interface Science*, 2018, **512**, P. 47–54.
- [9] Devi L.G., Kavitha R. Enhanced photocatalytic activity of sulfur doped TiO₂ for the decomposition of phenol: A new insight into the bulk and surface modification. *Materials Chemistry and Physics*, 2013, **143**(3), P. 1300–1308.
- [10] Zhang J., Chen X., Shen Y., Li Y., Hu Z., Chu J. Synthesis, surface morphology, and photoluminescence properties of anatase iron-doped titanium dioxide nano-crystalline films. *Phys. Chem. Chem. Phys.*, 2011, **13**, P. 13096–13105.
- [11] Abazovic N.D., Comor M.I., Dramicanim M.D., Jovanovic D.J., Ahrenkiel S.P., Nadeljkovic J.M. Photoluminescence of anatase and rutile TiO₂ particles. *J. Phys. Chem. B*, 2006, **110**, P. 25366–25370.
- [12] Mathew S., Prasad A.K., Benoy T., Rakesh P.P., Hari M., Lishish T.M. UV-Visible photoluminescence of TiO₂ nanoparticles prepared by hydrothermal method. *J. Fluoresc.*, 2012, **22**, P. 1593–1599.
- [13] Zhang H., Zhou M., Fu Q., Lei B., Lin W., Guo H., Wu M., Lei Y. Observation of defect state in highly ordered titanium dioxide nanotube arrays. *Nanotechnology*, 2014, **25**(27), P. 275603.
- [14] Chetibi L., Busko T., Kulish N.P., Hamana D., Chaieb S., Achour S. Photoluminescence properties of TiO₂ nanofibers. *J. Nanopart. Res.*, 2017, **19**, P. 129.
- [15] Tsai C.T., Chuu D.S., Chen G.L., Yang S.L. Studies of grain size effects in rf sputtered CdS thin films. *J. Appl. Phys.*, 1996, **79**(12), P. 9105–9109.
- [16] Yang Y., Chen H., Mei Y., Chen J., Wu X., Bao X. CdS nanocrystallinities prepared by chemical and physical templates. *Acta Materialia*, 2002, **50**, P. 5085–5090.
- [17] Kumar P., Saxena N., Singh F., Agarwal A. Nanotwinning in CdS quantum dots. *Physica C*, 2012, **407**, P. 3347–3351.
- [18] Abken A.E., Halliday D.P., Durose K. Photoluminescence study of polycrystalline photovoltaic CdS thin film layers grown by close-spaced sublimation and chemical bath deposition. *J. Appl. Phys.*, 2009, **105**, P. 064515.
- [19] Jin C., Liu B., Lei Z., Sun J. Structure and photoluminescence of the TiO₂ films grown by atomic deposition using tetrakis-dimethylamino titanium and ozone. *Nanoscale Research Letters*, 2015, **10**(1), P. 95.
- [20] Han S., Pu Y.-C., Zheng L., Zhang J., Fang X. Shell-thickness dependent electron transfer and relaxation in type-II core-shell CdS/TiO₂ structures with optimized photoelectrochemical performance. *J. Materials Chem. A*, 2015, **3**, P. 22627–22635.
- [21] Li X., Xia T., Xu C., Murowchick J., Chen X. Synthesis and photoactivity of nanostructured CdS-TiO₂ composite catalysts. *Catalysis Today*, 2014, **225**, P. 64–73.
- [22] Thakur P., Chadha R., Biswas N., Sarkar S.K., Mukherjee T., Joshi S.S., Kapoor S. Synthesis and characterization of CdS doped TiO₂ nanocrystalline powder: A spectroscopic study. *Materials Research Bulletin*, 2012, **47**, P. 1719–1724.
- [23] Guo X., Chen C., Song W., Wang X., Di W., Qin W. CdS embedded TiO₂ hybrid nanospheres for visible light photocatalysis. *J. Molecular Catalysis A: Chemical*, 2014, **387**, P. 1–6.

- [24] Vorokh A.S., Kozhevnikova N.S., Gorbunova T.I., Gyrdasova O.I., Baklanova I.V., Yanchenko M.Yu., Myrzakaev A.M., Shalaeva E.V., Enyashin A.N. Facile, rapid and efficient doping of amorphous TiO₂ by pre-synthesized colloidal CdS quantum dots. *J. Alloys and Comp.*, 2017, **706**, P. 205–214.
- [25] Ulyanova E.S., Zamyatin D.A., Murzakaev A.M., Yushkov A.A., Kozhevnikova N.S., Gorbunova T.I., Vorokh A.S., Enyashin A.N., Shalaeva E.V. Local environment of CdS nanoparticles incorporated into anatase/brookite matrix via sol-gel route: HRTEM, Raman spectroscopy and MD simulation. *Materials Today Communications*, 2020, **25**, P. 101465.
- [26] Kozhevnikova N.S., Ulyanova E.S., Shalaeva E.V., Zamyatin D.A., Bokunyaeva A.O., Yushkov A.A., Kolosov V.Yu., Buldakova L.Yu., Yanchenko M.Yu., Gorbunova T.I., Pervova M.G., Enyashin A.N., Vorokh A.S. Low-temperature sol-gel synthesis and photoactivity of nanocrystalline TiO₂ with the anatase/brookite structure and an amorphous component. *Kinetics and Catalysis*, 2019, **60**, P. 325–336.
- [27] <http://powdercell-forwindows.software.informer.com/2.4>
- [28] Vorokh A.S., Rempel A.A. Direct-space visualization of the short and “average” long-range orders in the nanocrystalline structure of a single cadmium sulfide nanoparticle. *JETP Letters*, 2010, **91**(2), P. 100–104.
- [29] Kuznetsova Yu.V., Letofsky-Papst I., Sochor B., Schummer B., Sergeev A.A., Hofer F., Rempel A.A. Greatly enhanced luminescence efficiency of CdS nanoparticles in aqueous solution. *Colloids and Surfaces A*, 2019, **581**, P. 123814.
- [30] Iliev M.N., Hadjiev V.G., Litvinchuk A.P. Raman and infrared spectra of brookite (TiO₂): Experiment and theory. *Vibrational spectroscopy*, 2013, **64**, P. 148–152.
- [31] Prabhy R., Khadar M.A. Study of optical phonon modes of CdS nanoparticles using Raman spectroscopy. *Bull. Mater. Sci.*, 2008, **31**, P. 511–515.
- [32] Vequizo J.M., Kamimura S., Ohno T., Yamakata A. Oxygen induced enhancement of NIR emission in brookite TiO₂ powders: comparison with rutile and anatase powders. *Phys. Chem. Chem. Phys.*, 2018, **20**, P. 3241–3248.